HHS Public Access

Author manuscript

Nature. Author manuscript; available in PMC 2019 March 01.

Published in final edited form as:

Nature. 2018 March 01; 555(7694): 61–66. doi:10.1038/nature25762.

Extreme disorder in an ultra-high-affinity protein complex

Alessandro Borgia[#1,*], **Madeleine B. Borgia**[#1], **Katrine Bugge**[#2], **Vera M. Kissling**[1], **Pétur O. Heidarsson**[1], **Catarina B. Fernandes**[2], **Andrea Sottini**[1], **Andrea Soranno**[1,3], **Karin J. Buholzer**[1], **Daniel Nettels**[1], **Birthe B. Kragelund**[2,*], **Robert B. Best**[4,*], and **Benjamin Schuler**[1,5,*]

[1]Department of Biochemistry, University of Zurich, Zurich, Switzerland [2]Structural Biology and NMR Laboratory, The Linderstrøm-Lang Centre for Protein Science and Integrative Structural Biology at University of Copenhagen (ISBUC), Department of Biology, University of Copenhagen, Copenhagen, Denmark [3]Department of Biochemistry and Molecular Biophysics, Washington University School of Medicine, St. Louis, Missouri, 63110, USA [4]Laboratory of Chemical Physics, National Institute of Diabetes and Digestive and Kidney Diseases, National Institutes of Health, Bethesda, USA [5]Department of Physics, University of Zurich, Zurich, Switzerland

[#] These authors contributed equally to this work.

Summary

Molecular communication in biology is mediated by protein interactions. According to the current paradigm, the specificity and affinity required for these interactions are encoded in the precise complementarity of binding interfaces. Even proteins that are disordered under physiological conditions or contain large unstructured regions commonly interact with well-structured binding sites on other biomolecules. Here we demonstrate the existence of an unexpected interaction mechanism: The two intrinsically disordered human proteins histone H1 and its nuclear chaperone prothymosin α associate in a complex with picomolar affinity, but they fully retain their structural disorder, long-range flexibility, and highly dynamic character. Based on the close integration of experiments and molecular simulations, we show that the interaction can be explained by the large opposite net charge of the two proteins without requiring defined binding sites or interactions between specific individual residues. Proteome-wide sequence analysis suggests that this interaction mechanism may be surprisingly abundant in eukaryotes.

In the conventional paradigm of structural biology, intermolecular interactions are encoded in the complementary shapes and noncovalent forces between folded biomolecules. However, it has become increasingly clear that many proteins involved in cellular

[*]Correspondence should be addressed to B.S. (schuler@bioc.uzh.ch), A.B. (a.borgia@bioc.uzh.ch), R.B.B. (robertbe@helix.nih.gov). or B.B.K. (bbk@bio.ku.dk).

Author contributions

A.B., M.B.B., K.B., B.B.K., R.B.B., and B.S. designed and supervised research; M.B.B., A.B., V.K., and A.Sot. produced and labeled fluorescent protein variants; A.B. and M.B.B. performed single-molecule experiments; A.B., M.B.B., A.Sor., and D.N. analyzed single-molecule data; D.N. developed single-molecule instrumentation and data analysis tools; A.Sot. and A.B. carried out stopped-flow measurements, A.B., M.B.B., K.J.B., and A.Sot. established experimental conditions for single-molecule measurements; C.B.F., and P.O.H. produced protein samples for NMR; K.B. and C.B.F. performed and analyzed NMR measurements; A.Sor. carried out the bioinformatics analysis; R.B.B. conducted and analyzed simulations; A.B., B.B.K. and C.B.F. carried out CD experiments; B.S., A.B., R.B.B., B.B.K. and K.B. wrote the paper with the help from all authors.

interactions are fully or partially unstructured under physiological conditions[1,2]. In some cases, these intrinsically disordered proteins (IDPs) form a well-defined 3D-structure upon target binding[1]; in others, parts of the complex remain disordered. A broad spectrum of such protein complexes with different degrees of disorder are known[3]: Sometimes, a well-defined and structured binding interface is formed in the bound state, and only some loops or the chain termini stay disordered. In other cases, one of the binding partners remains almost completely unstructured in the complex, and its multiple binding motifs dynamically interact with the folded partner. Examples include interdomain interactions in the cystic fibrosis transmembrane regulator[4]; the cyclin-dependent kinase inhibitor Sic1 binding to the substrate recognition subunit of its ubiquitin ligase subunit Cdc4[5]; the tail of human Na^+/H^+ exchanger 1 with the extracellular signal-regulated kinase ERK2[6]; or nuclear transport receptors interacting with nucleoporins[7]. The underlying multivalent binding enables unique regulatory mechanisms[8] and can mediate the formation of liquid-liquid phase separation[9], indicating the emergence of new modes of biomolecular interactions.

We have discovered a pair of proteins that constitutes an extreme case of a highly unstructured protein complex with physiological function. One binding partner, the linker histone H1.0 (H1), which is involved in chromatin condensation by binding to nucleosomes[10,11], is largely unstructured[12] and highly positively charged, with two disordered regions flanking a small folded globular domain (Fig. 1, Extended Data Table 1). The other partner, the abundant nuclear protein prothymosin α (ProTα), is a fully unstructured, highly negatively charged IDP[13,14] involved in chromatin remodeling[15], transcription, cellular proliferation, and apoptosis[16]. ProTα acts as a linker histone chaperone by interacting with H1 and increasing its mobility in the nucleus[17]. We show here that ProTα and H1 bind to each other with very high affinity, but both proteins fully retain their structural disorder. Based on the integration of complementary experimental techniques and molecular simulations, we obtain a detailed model of this highly disordered and dynamic protein complex, which represents a new paradigm of biomolecular binding.

An extremely unstructured protein complex

The binding of H1 to ProTa has been demonstrated both *in vitro*[18] and *in vivo*[11]. However, their high net charge, low hydrophobicity, and pronounced disorder in the free proteins raise the question of how much structure is formed when they interact. We used circular dichroism (CD) and nuclear magnetic resonance (NMR) spectroscopy to investigate the formation of secondary and tertiary structure. The CD spectra of unbound ProTα and H1 reflect the low secondary structure content of the individual IDPs, except for the small helix-turn-helix domain of H1[13,19,20] (Fig. 1c). Surprisingly, the CD spectrum of an equimolar mixture of the two proteins can be explained by the simple sum of the individual spectra, indicating that complex formation entails minimal changes in average secondary structure content.

To obtain residue-specific information, we employed NMR spectroscopy. ^1H,^{15}N heteronuclear single quantum coherence (HSQC) spectra of the individual proteins exhibit low dispersion of the ^1H chemical shifts, as expected for IDPs[14,21-23] (Fig. 1e,f). Only the globular domain of H1, which is stably folded even in isolation (Extended Data Fig. 1),

shows the large dispersion of resonances characteristic of tertiary structure[23,24] (Fig. 1g). Remarkably, the overall peak dispersion remains unchanged upon complex formation, confirming that no pronounced tertiary structure is formed upon binding. Nevertheless, small but clearly detectable peak shifts observed for ProTα and H1 indicate significant changes in the average chemical environment of the corresponding residues, as expected upon interaction with the large opposite charge of the other IDP. For ProTα, 95% of the amide backbone nuclei could be assigned (Extended Data Fig. 2), enabling a residue-specific analysis: The C^{α} secondary chemical shifts[25] of ProTα show no evidence for the induction of persistent or transiently populated secondary structure upon complex formation (Fig. 1d), in agreement with the CD data (Fig. 1c). The severe overlap in the NMR spectra of the unstructured parts of H1 precluded residue-specific assignments, but the clusters of H^{α}-C^{α} peaks in the ^{1}H,^{13}C-HSQC spectrum from the lysine-rich disordered regions neither exhibit detectable chemical shift perturbations upon titration with ProTα, nor do additional resonances emerge (Extended Data Fig. 3e,f). We thus have no indications of changes in secondary structure content in H1 upon ProTα binding, even though we cannot exclude subtle structural adjustments within the uncertainty of the CD and NMR data.

The lower intensity of the resonances corresponding to the H1 globular domain (Fig. 1f,g, Extended Data Fig. 3) is likely to originate from the faster transverse (T2) relaxation of structured compared to unstructured regions; additionally, tumbling of the globular domain is decelerated by the drag of the unstructured regions it is embedded in[26]. Upon complex formation, the intensity of many H1 (and ProTα) resonances decreases, and those of the globular domain drop below the noise (Extended Data Fig. 3b and Fig. 1f,g). The large hydrodynamic radii of H1 and the complex (Extended Data Fig. 4a,b) support a large effective rotational correlation time as the origin of peak broadening, but an additional contribution from chemical exchange cannot be excluded. Note, however, that the globular domain is dispensable for complex formation (Fig. 2b, cf. *High-affinity binding in spite of disorder*).

High-affinity binding in spite of disorder

To quantify the strength of the interaction between H1 and ProTα, we used single-molecule Forster resonance energy transfer (FRET), which enables measurements over a very broad range of affinities, down to the picomolar regime. By labeling two positions with a donor and an acceptor dye, site-specific distances and distance changes between or within the polypeptides can be determined by confocal fluorescence detection of molecules freely diffusing in solution[27,28]. ProTα labeled at positions 56 and 110 exhibits a mean transfer efficiency, $\langle E \rangle$, of 0.33 at near-physiological ionic strength (Fig. 2a, Extended Data Table 2), as expected for this IDP, which is highly expanded owing to its large negative net charge[13,29,30]. Upon addition of unlabeled H1, a population with higher $\langle E \rangle$ of 0.58 (i.e. shorter average distance) emerges: Evidently, binding the positively charged H1 leads to a marked compaction of ProTα by charge screening, analogous to that obtained upon addition of salt[29]. The same behavior is observed for doubly labeled H1 (Extended Data Table 2), demonstrating a mutual adaptation of the conformational ensembles. The resulting dissociation constant in the low picomolar range reveals an extremely strong interaction with H1 (Fig. 2b, Extended Data Table 2), consistent with the physiological role of ProTα as a

linker histone chaperone[17] that needs to compete with the tight binding of H1 to chromatin[31]. Measurements with other FRET dyes and label positions resulted in very similar affinities (Extended Data Table 2), indicating that fluorescent labeling has only a small effect on binding. The dominant contribution to the interaction with ProTα stems from the unstructured C-terminal part of H1, which alone binds with picomolar affinity. The N-terminal half and the isolated globular domain of H1 also bind ProTα, but with much lower affinity (Fig. 2b). At least four isolated globular domains can bind to ProTα at the same time, with modest chemical shift changes (Extended Data Fig. 1), suggesting the absence of a specific binding interface.

The large and opposite net charges of ProTα (−44) and H1 (+53) imply a strong electrostatic contribution to binding. Indeed, a mere doubling of the ionic strength from the physiological 165 mM to 340 mM reduces the affinity by six orders of magnitude (Fig. 2c). By extrapolation, a reduction of ionic strength to ~140 mM would take this interaction into the femtomolar range. From low picomolar to 100 μM protein concentrations, the stoichiometries obtained from intermolecular FRET (Extended Data Fig. 4c) and NMR chemical shift titrations (Extended Data Figs. 2 and 3), as well as the hydrodynamic radii measured with pulsed-field gradient NMR and two-focus fluorescence correlation spectroscopy (2f-FCS) (Extended Data Fig. 4a,b) indicate the predominant formation of one-to-one dimers and the absence of large oligomers or coacervates[32]. However, in the presence of a large excess of one of the binding partners, a decrease in FRET efficiencies is indicative of the weak association of additional molecules with a K_D in the 10 to 100 μM range (Extended Data Fig. 4d,e). A weak propensity for trimer formation is also observed in the simulations described below (Extended Data Fig. 6).

A highly dynamic complex

The lack of structure formation in the H1-ProTα complex implies great flexibility and a highly dynamic interconversion within a large ensemble of configurations and relative arrangements of the two IDPs. The presence of a broad, rapidly sampled distance distribution is also supported by the analysis of fluorescence lifetimes[28,33,34] (Extended Data Fig. 5). Since fluctuations in distance cause fluctuations in the fluorescence intensity of donor and acceptor, the timescale of these long-range distance dynamics can be measured by single-molecule FRET combined with nanosecond fluorescence correlation spectroscopy (nsFCS)[34,35]. For individual unfolded or disordered proteins, reconfiguration times (inter-dye distance relaxation times) between ~20 ns and ~200 ns have been observed[27]. ProTα alone, with its highly expanded chain[13,29] and corresponding lack of impeding intramolecular interactions[36], is a particularly dynamic IDP and yields reconfiguration times, τ_r, between 29^{+2}_{-2} ns and 78^{+15}_{-9} [5] ns, depending on the chain segment probed[34,36] (Extended Data Table 2). H1 (labeled at positions 113 and 194) reconfigures more slowly, with $\tau_r = 118^{+24}_{-14}$ ns, but within the range previously observed for unfolded and intrinsically disordered proteins[27,34].

Strikingly, these pronounced and rapid long-range dynamics are retained in the complex, with values of τ_r between 66^{+2}_{-2} ns and 191^{+22}_{-19} ns for 13 different labeling pairs throughout

the dimer (Fig. 3a-d, Extended Data Table 2). The similarity of τ_r for the two proteins in the complex suggests a coupling of the dynamics of the two intertwining chains. The highly dynamic nature of the complex is further supported by NMR: The longitudinal (T_1) and transverse (T_2) ^{15}N relaxation times reflect rapid backbone dynamics in the pico- to nanosecond range, both for free ProTα and in the complex (Fig. 3h, Extended Data Fig. 2). The increase in T_1/T_2 (Fig. 3h) and R_H (Extended Data Fig. 4), and the reduced peak intensities (Fig. 3f) are consistent with the increase in τ_r for ProTα observed by nsFCS in the complex (Fig. 3a), where chain-chain interactions are expected to moderate both local and long-range dynamics.

Architecture of an unstructured protein complex

To develop a structural representation of the conformational ensemble of the H1-ProTα complex, we combine single-molecule FRET, NMR, and molecular simulations. We first map the complex with singlemolecule FRET by probing a total of 28 intra- and intermolecular distances with donor and acceptor dyes in specific positions (Figs. 3i, 4a). The resulting intermolecular transfer efficiencies lack pronounced patterns that would be expected for persistent site-specific interactions or an alignment of the chains in a preferred register. The intermolecular transfer efficiencies are most sensitive to the labeling position on ProTα, with the highest efficiencies (i.e. shortest average distances) for the central position ProTα 56, intermediate efficiencies for ProTα 110, and lowest efficiencies (i.e. longest distances) for ProTα 2. These results indicate that the region of highest charge density of ProTα (Fig. 1b) most strongly attracts the oppositely charged polypeptide chain of H1. The charge density along H1 is more uniform (Fig. 1a), as are the transfer efficiencies to ProTα, with only a slight decrease towards the termini (Fig. 3i).

Based on this information, we sought to establish a molecular model of the H1-ProTα complex. Given the lack of specific structure formation and residue-specific interactions, the dominance of electrostatics in the complex, and the size of the system, we used a simplified model in which each residue is coarse grained into a single bead. Coulombic interactions between all charged residues are explicitly included, with a screening factor to account for buffer ions, representing an ionic strength of 165 mM. Other attractive interactions as well as excluded volume repulsion are captured via a short-range potential, with the radius of the residues determined from their volumes[37]. A structure-based potential[38] is used to describe the folded globular domain of H1. The transfer efficiencies computed from Langevin dynamics simulations can be matched to the measured values (Fig. 4a) via the single adjustable parameter in our model, namely the contact energy of the short-range potential, which is the same for all residues (see Methods); explicitly including a representation of the chromophores in the simulations yielded very similar results (Fig. 4a). The resulting intra- and intermolecular distance distributions (Extended Data Fig. 6d) are smooth and unimodal, in accord with the absence of site-specific interactions and lack of structure formation observed experimentally, and attesting to the convergence of the simulations. The good agreement between the transfer efficiency values from experiment and simulation indicates that this simple model, in which the only consequential difference between residues is their charge, captures the essential properties of the structural ensemble. Considering its simplicity, the femtomolar affinity estimated from the model (Extended Data Fig. 5b) is

remarkably consistent with the affinities observed experimentally near this ionic strength. Furthermore, the affinity for a second molecule of H1 or ProTα to the complex is predicted to be orders of magnitude weaker, consistent with experiment (Extended Data Figs. 4d,e and 6b).

The resulting intra- and intermolecular distance maps (Fig. 4b) indicate that the interactions between ProTα and H1 are broadly distributed along their sequences, but they also reflect the asymmetry in electrostatic attraction owing to the higher charge density of ProTα in its central and C-terminal regions, as revealed by the single-molecule experiments (Fig. 4a). The NMR results provide an independent experimental test of the model: Indeed, the distribution of the average number of contacts made by the residues of ProTα based on the simulation (Fig. 3e) is strikingly similar to the distribution of changes in chemical shifts, peak intensities, and T_1/T_2 ratios observed upon binding (Fig. 3f-h). These changes occur across the same broad region between residues 46 and 106, encompassing the most acidic tracts of ProTα. Even though peak overlap in clusters of Glu residues prevents a quantitative analysis for some residues in this region, these resonances are not broadened beyond detection, as might be expected for persistent interactions.

Further analysis of the simulated structural ensemble shows a lack of identifiable distinct clusters of configurations (Extended Data Fig. 6a), implying a continuous, unimodal structure distribution. A projection of the simulation onto the first three principal components of the inter-residue distances (Extended Data Fig. 6c) reveals a highly heterogeneous ensemble of arrangements with a wide variety of configurations of the two entwining chains (Fig. 4c). Given the rapid intramolecular dynamics and lack of structure in the complex, the activation barrier for binding is likely to be close to zero. Indeed, association of H1 and ProTα occurs at the diffusion limit, with a binding rate coefficient of $(3.1 \pm 0.1) \cdot 10^9\ M^{-1}s^{-1}$ (Extended Data Fig. 7). The simulations support this mechanism, with a downhill free energy surface for binding, and attractive fly-casting[39] interactions enhanced by electrostatics[40] emerging already at a distance of ~22 nm, much greater than the sum of the hydrodynamic radii (Extended Data Fig. 6b).

Conclusions

Our results suggest that high-affinity complex formation between two oppositely charged IDPs is possible without the formation of structure or the need for folded domains. In contrast to the prevalent paradigm of molecular recognition in biomolecular interactions, this type of highly dynamic complex does not require structurally defined binding sites or specific persistent interactions between individual residues. Rather, the results are well described by long-range electrostatic attraction between the two interpenetrating polypeptide chains, especially between their charge-rich regions. The exceedingly rapid interconversion of many different arrangements and configurations on the 100-ns timescale results in efficient averaging and thus a mean-field-type interaction[41,42] between all charges. This type of complex further expands the known spectrum of disorder in protein-protein interactions[3]. Although the complex of H1 and ProTα is extreme in its extent of disorder retained for both binding partners, the possibility of this interaction mechanism may not be entirely unexpected, given the prevalence of charged amino acids in many IDPs[2], the previous

observation of disorder in IDPs interacting with folded proteins[4-7], and the role of electrostatics in the formation of dynamic binding interfaces between folded proteins[43]. Moreover, the H1-ProTα interaction resembles polyelectrolyte complexes formed by charged synthetic polymers[42], even though the latter usually phase-separate into coacervates. The absence of coacervation[32,42] or liquid-liquid phase separation[9] for ProTα and H1 at concentrations from picomolar to high micromolar may be due to the complementarity[44] of the two proteins in terms of effective length and opposite net charge, leading to optimal, mutually saturating electrostatic interactions, or the lack of hydrophobic and aromatic side chains and cation-π interactions, which have been suggested to favor phase separation mediated by proteins[32,45,46].

What are the functional implications of such a high-affinity yet unstructured dynamic complex between two IDPs? Histone H1 is a key factor in chromatin condensation and transcriptional regulation[11], and ProTα acts as a chaperone of H1 that facilitates its displacement from and deposition onto chromatin[17]. ProTα thus needs to be able to compete with the very high affinity of the histone to chromatin[31]. However, high affinities between structured biomolecules are usually linked to exceedingly slow dissociation[40], incompatible with fast regulatory response. By contrast, the high affinity of the H1-ProTα complex is facilitated by its ultra-fast association, which enables dissociation on a biologically useful timescale in spite of the high affinity required for function. Another consequence of polyelectrolyte interactions is the possibility of ternary complex formation[47], signs of which are detected here with a large excess of ProTα or H1 (Extended Data Figs. 4d,e and 6b), resulting in largely unexplored kinetic mechanisms that cannot be explained by competition via simple dissociation and re-association[48]. Finally, the flexibility within such unstructured complexes may facilitate access for enzymes adding posttranslational modifications, which play key roles in the regulation of cellular processes, including those of H1. Another example of this mechanism may be the interaction of the acidic domain of the oncogene SET with the lysine-rich C-terminal tail of p53, which is regulated by acetylation[49].

The behavior we observe for ProTα and H1 might be surprisingly widespread, since highly charged protein sequences that could form such complexes are abundant in eukaryotes. In the human proteome alone, several hundred proteins that are predicted to be intrinsically disordered[50] contain contiguous stretches of at least 50 residues with a fractional net charge similar to that of H1 or ProTα. Since the interaction of highly oppositely charged IDPs is unlikely to be very sequence-specific[18], achieving binding selectivity may be linked to other regulatory mechanisms, e.g. cellular localization or synchronized expression during relevant stages of development or the cell cycle.

Extended Data

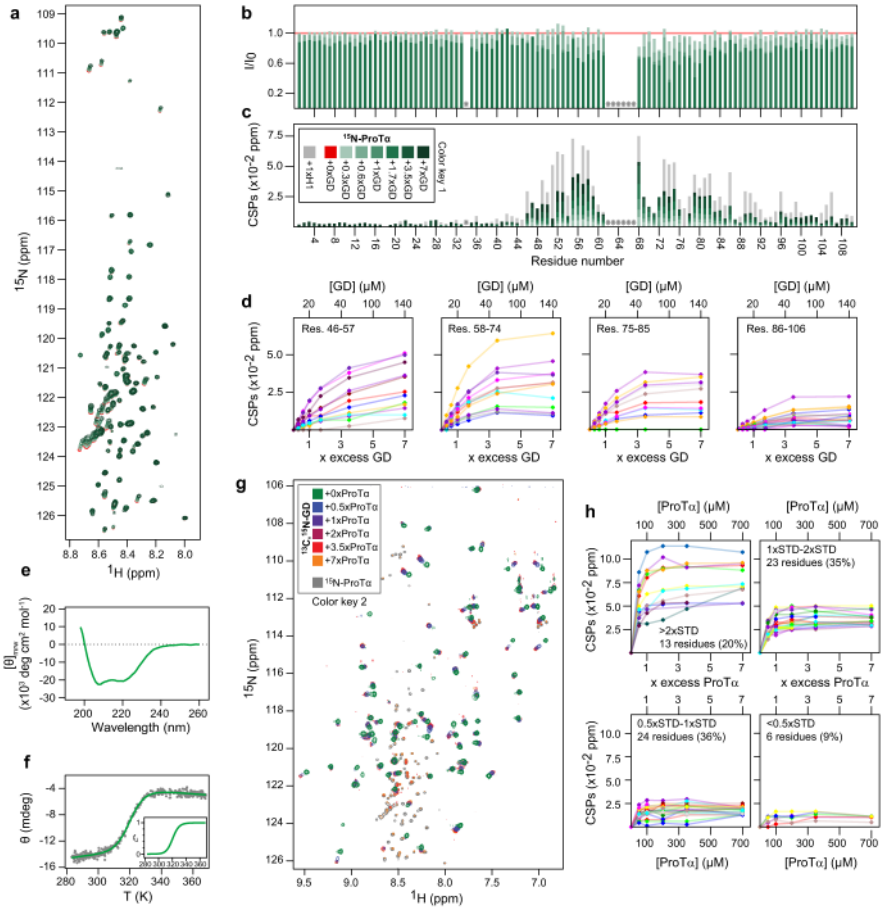

Extended Data Figure 1. Titrations of ProTα and Globular Domain (GD).

(a) Titration of ^{15}N-ProTα with 0- to 7-fold molar addition of GD followed by ^{1}H,^{15}N-HSQC spectra. **(b)** Peak intensity ratios for assigned residues of ProTα relative to the free state induced by 0- to 1.7-fold molar addition of GD. **(c)** CSPs per residue of ProTα induced by 0- to 7-fold molar addition of GD. For comparison, CSPs of ProTα upon 1-fold molar addition of H1 are shown in grey. Panels **a-c** follow color key 1; light grey stars indicate prolines and unassigned residues. **(d)** ProTα CSPs plotted against concentration and times excess of GD relative to the free state for residues 46-106 upon 0- to 7-fold molar addition of GD. Colors used for discriminability. **(e)** Far-UV CD spectrum of GD. **(f)** Thermal denaturation of GD followed by the change in ellipticity at 222 nm (T_m = 320.5 ± 0.3 K, ΔH_m = −44 ± 2 kcal mol^{-1}). Insert: Fraction unfolded GD (f_u) as a function of temperature. **(g)** Titration of 100 μM ^{13}C,^{15}N-GD with 0- to 7-fold molar addition of ProTα followed by ^{1}H,^{15}N-HSQC spectra (color key 2). Peak intensities gradually decrease during the titration. At 3.5×- and 7× excess ProTα, natural abundance peaks of free ProTα appear (^{1}H,^{15}N-HSQC spectrum of ^{15}NProTα shown in grey for comparison). **(h)** CSPs of GD plotted against concentration and times excess of ProTα relative to the free state upon 0- to 7-fold molar addition of ProTα. A total of 66 (unassigned) amide backbone peaks were followed

and grouped according to the standard deviation (STD) of the CSPs (1 STD = 0.0254 ppm). Of these, 55% had CSPs larger than 1 STD. Colors used for discriminability.

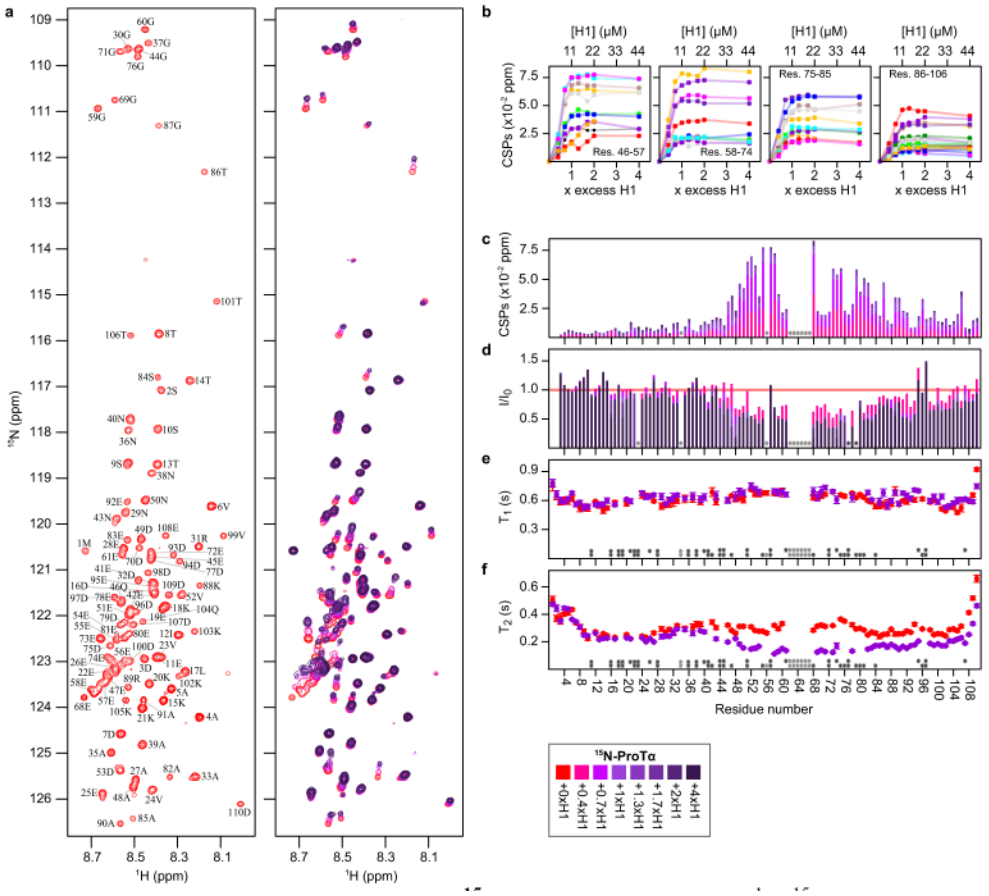

Extended Data Figure 2. Titration of ^{15}N-ProTα with H1.

(a) ^{1}H,^{15}N-HSQC spectrum of 11 μM free ^{15}NProTα with residue labels (left) and titrated with 0- to 4-fold molar addition of H1 (right) (see color key). **(b)** Weighted backbone amide chemical shift perturbations (CSPs) of ProTα (residues 46-106) relative to the free state upon 0- to 4-fold molar addition of H1, plotted against concentration and times excess of H1. Colors used for discriminability. **(c)** CSPs and **(d)** peak intensity ratios for assigned residues of ProTα induced by 0- to 4-fold molar addition of H1 (for bar colors, see key). **(e)** Longitudinal 15N relaxation times (T_1) of free (red) and H1-bound (purple) ^{15}N-ProTα. $\langle T_1 \rangle$ is 610 ms (free) and 636 ms (complex). **(f)** Transverse 15N relaxation times (T_2) of free (red) and H1-bound (purple) ^{15}N-ProTα. $\langle T_2 \rangle$ is 302 ms (free) and 217 ms (complex). In c-f, light grey stars indicate prolines and unassigned residues, dark grey stars overlap and/or insufficient data quality.

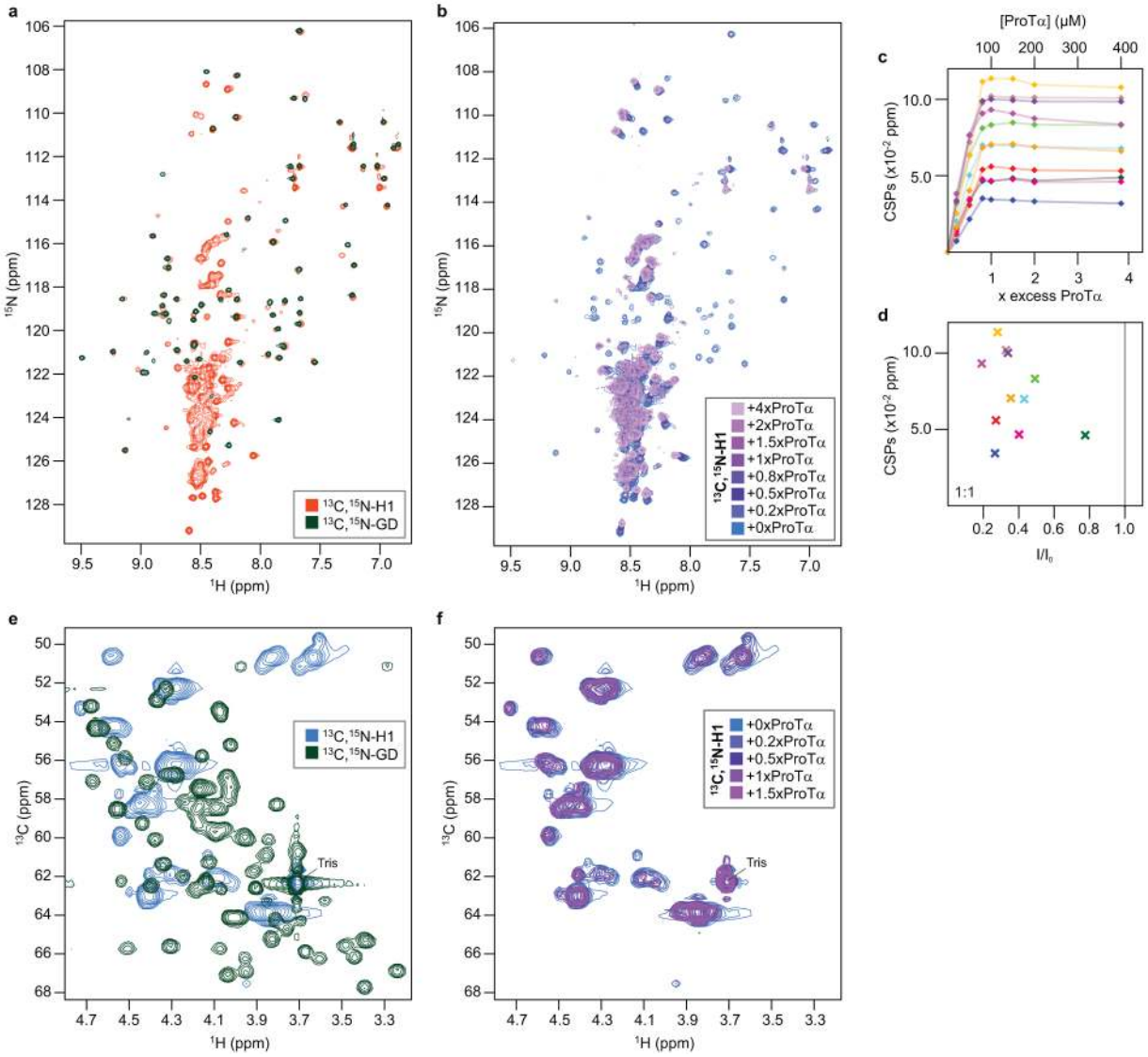

Extended Data Figure 3. Titration of ^{13}C,^{15}N-H1 with ProTα.

(a) ^{1}H,^{15}N-HSQC spectra of free ^{13}C,^{15}NGD (globular domain, dark green) and free ^{13}C, ^{15}N-H1 (orange). The majority of the amide peaks of the GD overlap with the more dispersed peaks from full-length H1, indicating the similarity in structure of the GD in isolation and within H1. (**b)** Titration followed by ^{1}H,^{15}N-HSQC spectra of ^{13}C,^{15}N-H1 with 0- to 4-fold molar addition of ProTα. Data acquired on His6-tagged H1. **(c)** CSPs relative to free H1 of eleven traceable H1 amide backbone peaks from the intrinsically disordered region (based on overlay with ^{1}H,^{15}N-HSQC spectra of GD (a)) upon 0 to 4-fold molar addition of ProTα plotted against concentration and times excess. Colors used for discriminability. **(d)** CSPs plotted against peak intensity ratios relative to the free state of H1 of the eleven H1 amides at 1× excess of ProTα. Colors as in (c). **(e)** Overlay of C^{α},H^{α} region from ^{1}H,^{13}C-HSQC spectra of free ^{13}C,^{15}N-H1 (blue) and ^{13}C,^{15}N-GD (green). The H1 ^{1}H,^{13}C-HSQC is dominated by intense clusters of peaks not present in the GD spectrum, consistent with the large fraction of repeats in the H1 disordered regions. **(f)** C^{α},H^{α} region

of ^{13}C,^{15}N-H1 upon titration with ProTα. The lack of detectable changes in C^{α},H^{α} resonances is consistent with the absence of secondary structure induction in the disordered regions of H1 upon binding.

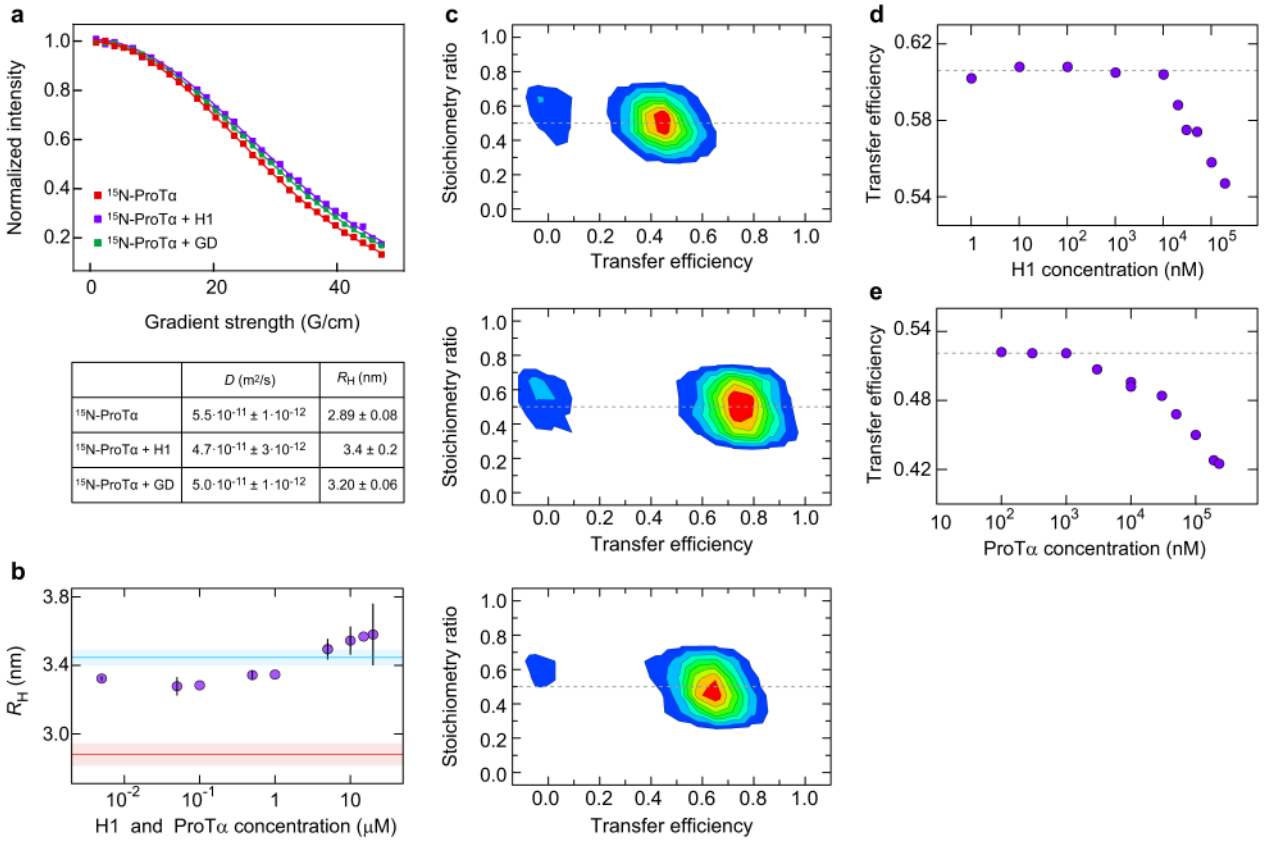

Extended Data Figure 4. Hydrodynamic radii and stoichiometry of the H1-ProTα complex.

(a) Hydrodynamic radii, R_H, of free and bound ^{15}N-ProTα (100 μM) determined with pulsed-field gradient NMR at 283 K. The signal decays of free ^{15}N-ProTα (red), with H1 at a 1:1 molar ratio (purple), and with H1 GD at a 1:7 molar ratio (green) as a function of gradient strength, together with corresponding fits and a table of the diffusion coefficients and resulting R_H values. **(b)** R_H measured by 2f-FCS at 295 K. Lines show the R_H of H1 -1C (blue) and ProTα D2C (red) labeled with Alexa 594 in the absence of binding partner. Symbols show labeled ProTα (5 nM) in the presence of equimolar concentrations of unlabeled ProTα and unlabeled H1, with s.d.s indicated by error bars or shaded bands. **(c)** Stoichiometry ratio[71] versus transfer efficiency plots from intermolecular single-molecule FRET experiments with singly labeled protein variants as indicated in the panels. A stoichiometry ratio of 0.5 indicates a 1:1 complex. **(d,e)** Transfer efficiency changes at large excess of unlabeled binding partner for FRET-labeled ProTα C56C110 (d) and H1 C104C194 (e).

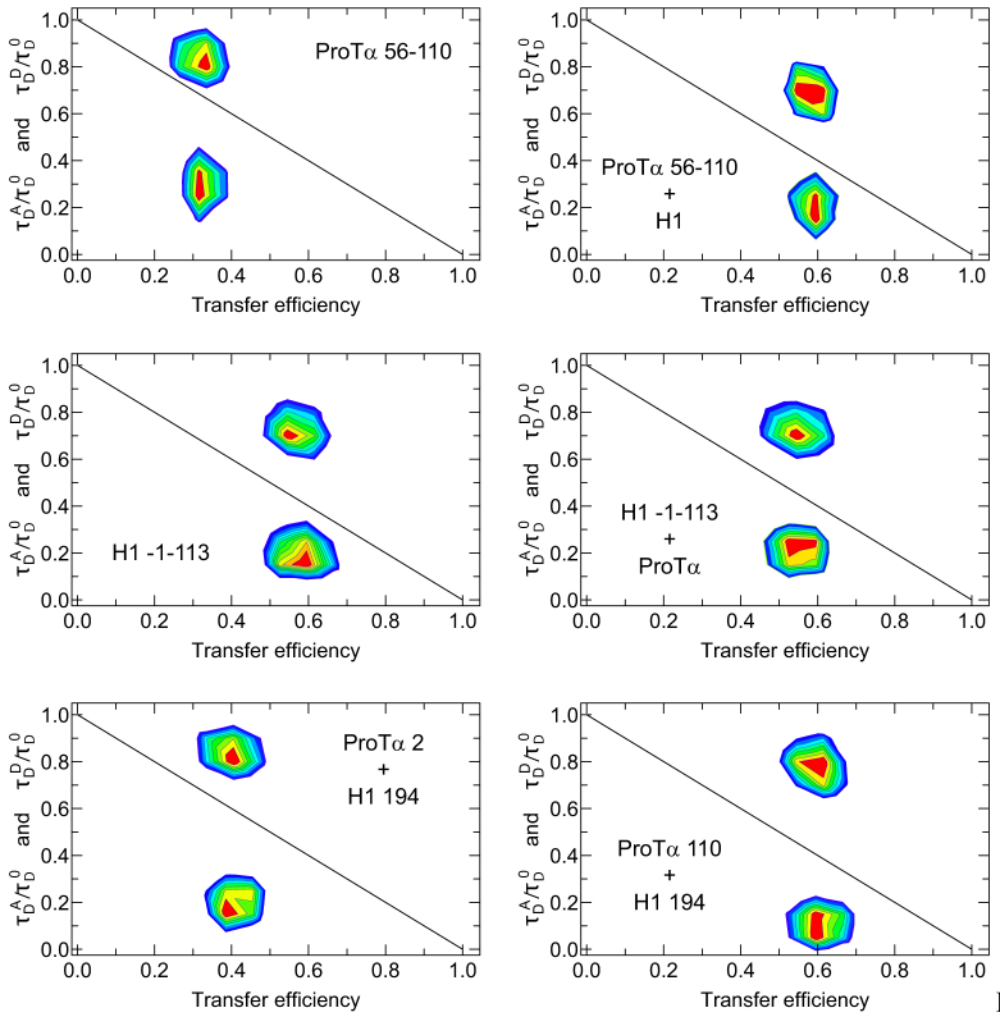

Extended Data Figure 5. Fluorescence lifetime analysis.

Plots of the fluorescence lifetimes of donor (Alexa 488),τ_D^D, and acceptor (Alexa 594),τ_D^A, normalized by the intrinsic donor lifetime, τ_D^0, versus the ratiometric transfer efficiency, E (calculated from the number of donor and acceptor photon counts), as a diagnostic for the presence of a broad distance distribution rapidly sampled during the time of a fluorescence burst [28, 33, 34]. If fluctuations in transfer efficiency occur on a timescale between the donor fluorescence lifetime (~4 ns) and the burst duration (~1 ms), the normalized donor lifetimes cluster above, and the acceptor lifetimes below the solid diagonal line expected for a single fixed distance, as previously observed for intrinsically disordered proteins [34, 72]. The large deviation from the diagonal observed for both unbound and bound ProTα and H1 supports the presence of broad, rapidly sampled distance distributions.

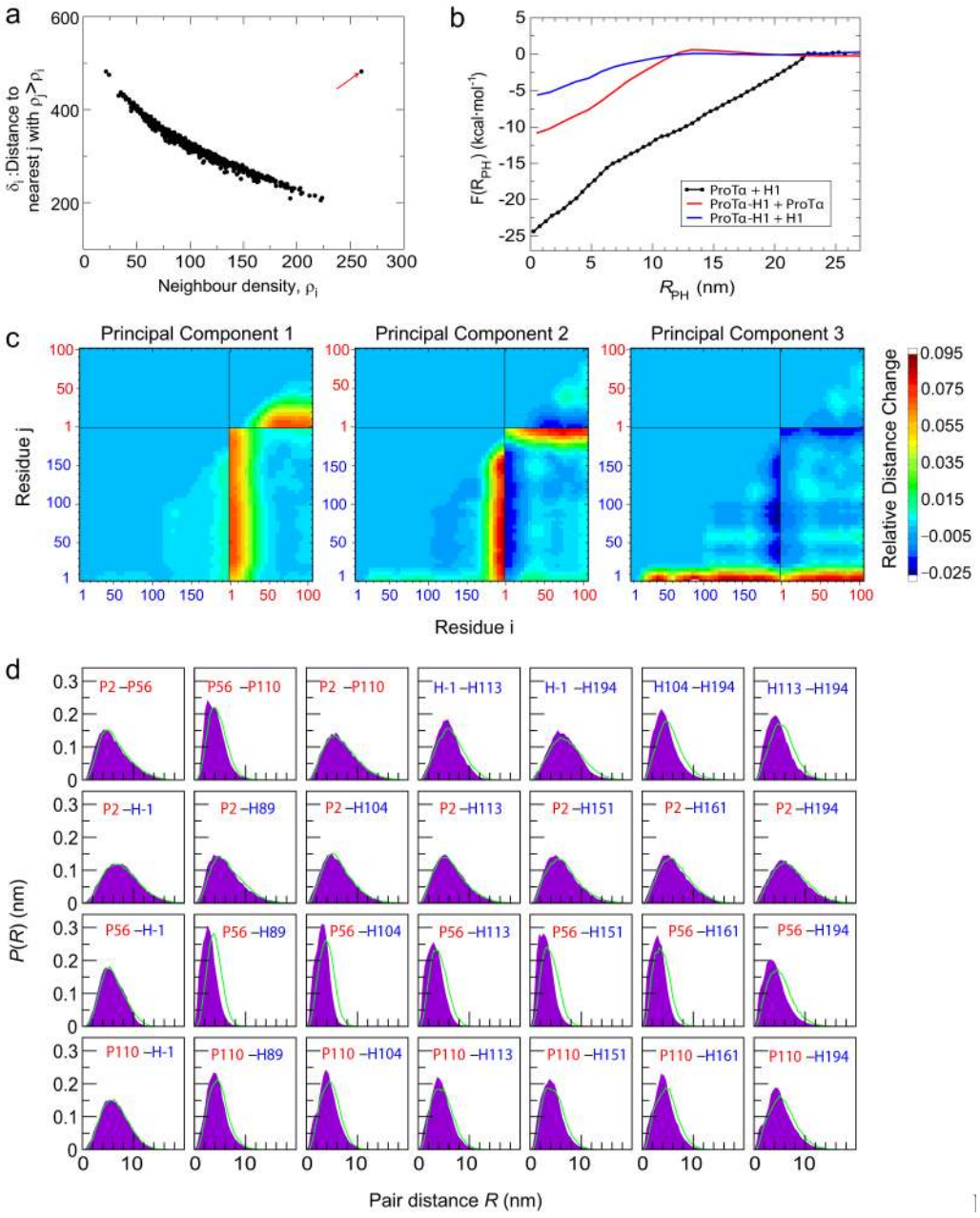

Extended Data Figure 6. Simulation results.

(a) Decision graph using the Rodriguez-Laio clustering algorithm[70], showing only a single density maximum distant from other density maxima, i.e. a single distinct cluster. **(b)** Free energy for association of ProTα and H1 from simulation, yielding a K_D of 7 fM at R_{PH} = 0 (black curve). Blue and red curves are the free energies for addition of a second H1 or a second ProTα, respectively, to an existing H1-ProTα complex. **(c)** Principal component (PC) vectors shown as contact maps. Colors indicate the increase or decrease in each pair distance for that PC, relative to the other distances. ProTα and H1 residue numbers are indicated in red and blue, respectively. Each PC describes a feature of the chain arrangement: PC1, e.g., captures the presence or absence of interactions between the ProTα

N-terminus and H1. **(d)** Intramolecular (top row) and intermolecular (rows 2 to 4) distributions of distances corresponding to FRET labeling sites, for the ProTα-H1 complex (labels P*X*-H*Y* refer to residues *X* and *Y* in ProTα and H1, respectively). Filled distributions: simulations without explicit chromophores; green lines: simulations with explicit chromophores.

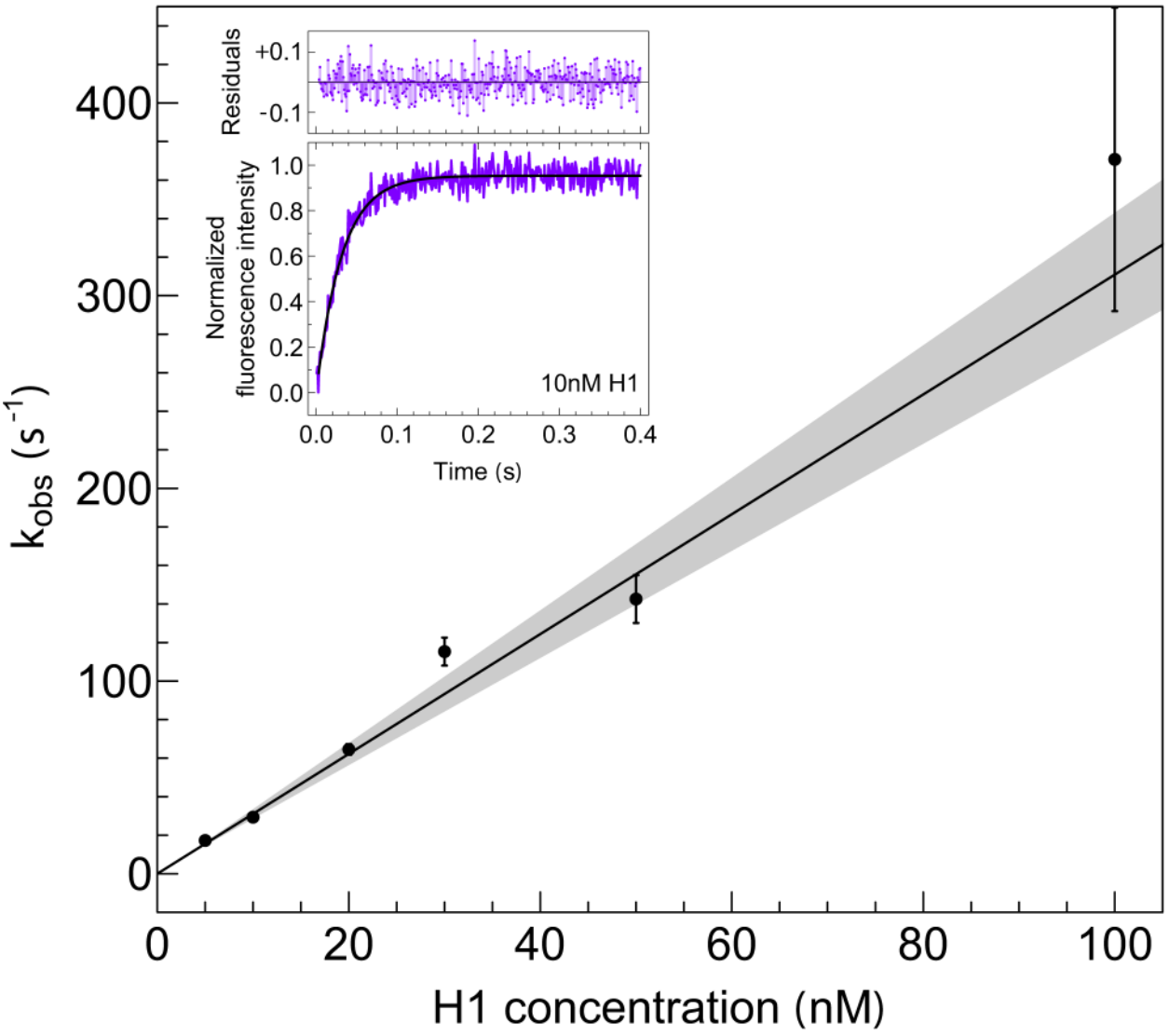

Extended Data Figure 7. Kinetics of H1-ProTα binding measured by stopped flow.

FRET-labeled ProTα 56-110 is mixed rapidly with unlabeled H1 in TBS buffer, and the resulting increase in acceptor fluorescence is monitored (inset, measured at 10 nM H1 with single-exponential fit and residuals above, see Methods for details). Decay rates were obtained from single-exponential fits, assuming an instrument dead time of 3 ms. Standard errors for each H1 concentration were obtained via bootstrapping. The observed rates, k_{obs}, are shown as a function of H1 concentration (c_{H1}); for H1 concentrations between 10 and 100 nM, where pseudo-first order conditions apply (ProTα concentration after mixing was 2 nM), they were fit with $k_{obs} = k_{on}c_{H1} + k_{off} = k_{on}c_{H1} + k_{on}k_D$, using the independently

determined K_D of 2.1 pM (Extended Data Table 2). The fit yields a bimolecular association rate coefficient of $k_{on} = (3.1 \pm 0.1) \cdot 10^9$ M^{-1} s^{-1} and an apparent dissociation rate coefficient of $k_{off} = (6.5 \pm 3.1) \cdot 10^{-3}$ s^{-1}. The gray area represents the 95% confidence band.

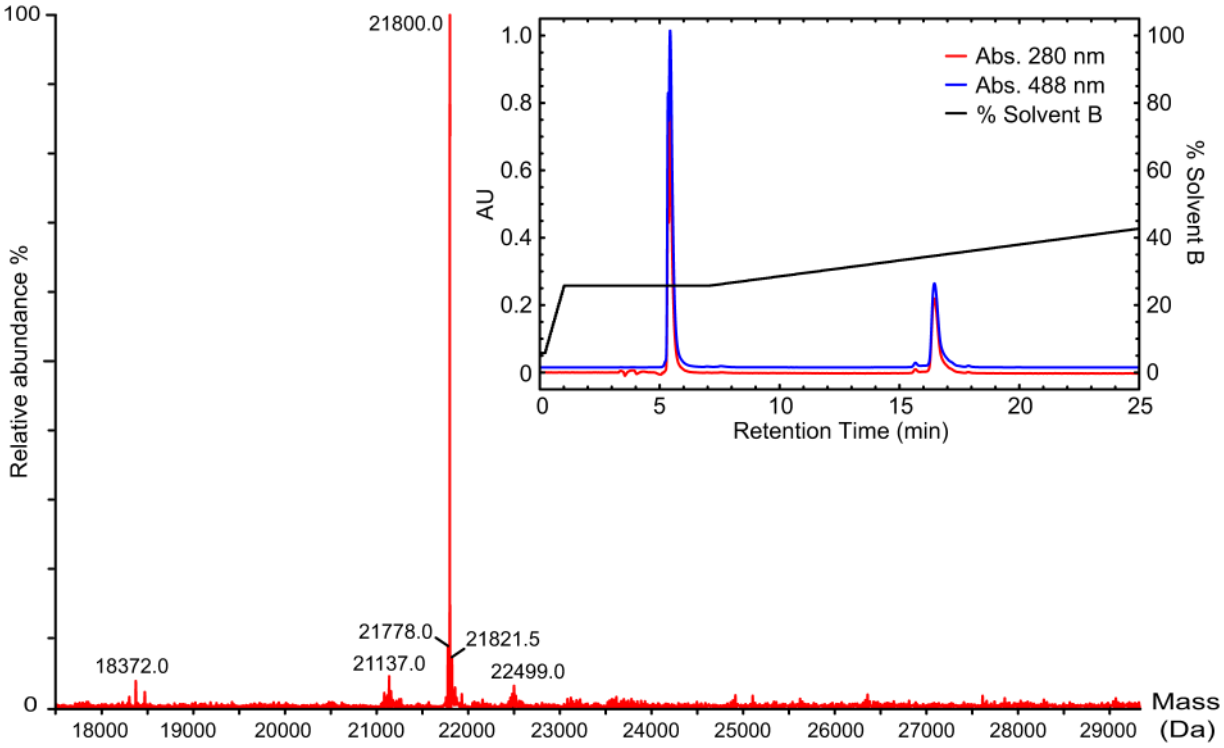

Extended Data Figure 8. Example of the quality of the H1 preparation.

Electrospray ionization mass spectrum of H1 T161C labeled with Alexa 488 (calculated mass 21,800 Da) and reversed-phase HPLC (Vydac C4) chromatogram (inset) showing absorption at 280 nm (red) and 488 nm (blue) and the elution gradient from solvent A (5% acetonitrile in H2O + 0.1% TFA) to solvent B (100% acetonitrile) (black), illustrating the high purity of the sample. The peak at ~5.5 min corresponds to free Alexa 488, the peak at ~16.8 min to H1 T161C labeled with Alexa 488.

Extended Data Table 1.

Sequences of protein constructs and fluorescently labeled variants of H1 and ProTα. **(top)** Sequences of H1 and ProTα wildtype and variants used. Bold yellow-shaded residues are positions mutated to Cys for fluorophore conjugation. Residues in red are part of protease recognition sites used to cleave the HisTag with thrombin (GGPR or GC) or HRV-3C (GP). (Note that the wt sequence of H1 starts with "T"; the preceding Cys residue (−1) was added for labeling.) The underlined H1 sequence indicates the globular domain (GD), identified based on a sequence alignment with the *G. gallus* homolog[20] (PDB access code 1HST, 82% sequence identity). Surface-exposed residues (as shown in Fig. 1a and 5b) are shaded in light blue. The net charge of each variant is indicated in parentheses. [a]C-

terminal disordered region. [b]N-terminal disordered region including GD. **(bottom)** Labeled variants of H1 and ProTα. [c]Förster radius of the corresponding dye pair.

H1 (+53)	-1 23 CTENSTSAPAAKPKRAKASKKSTDHPKYSDMIVAAIQAEKNRAGSSRQSIQKYIKSHYKVGENADSQI 89 96 104 113 KLSIKRLVTTGVLKQTKGVGASGSFRLAKSDEPKKSVAFKKTKKEIKKVATPKKASKPKKAASKAPTK 151 161 193 KPKATPVKKAKKKLATPKKAKKPKTVKAKPVKASKPKKAKPVKPKAKSSAKRAGKKKGGPR
H1 [a]CTR (+39)	103 SVAFKKTKKEIKKVATPKKASKPKKAASKAPTKKPKATPVKKAKKKLAATPKKAKKPKTVKAKPVKASK 193 PKKAKPVKPKAKSSAKRAGKKKGGPR
H1 [b]NTR (+18)	-1 GCTENSTSAPAAKPKRAKASKKSTDHPKYSDMIVAAIQAEKNRAGSSRQSIQKYIKSHYKVGENADSQI 113 KLSIKRLVTTGVLKQTKGVGASGSFRLAKSDEPKKSVAFKKTKKEI
GD (+9)	23 DHPKYSDMIVAAIQAEKNRAGSSRQSIQKYIKSHYKVGENADSQIKLSIKRLVTTGVLKQTKGVGASGS 96 FRLAK
ProTα (-44)	1 56 GPSDAAVDTSSEITTKDLKEKKEVVEEAENGRDAPANGNAENEENGEQEADNEVDEEEEEGGEEE 110 EEEEEGDGEEEDGDEDEEAESATGKRAAEDDEDDDVDTKKQKTDEDD

H1				ProTα				
Singly labeled		**Doubly labeled**		**Singly labeled**		**Doubly labeled**		
Alexa 488	Alexa 594	Alexa 488/ Alexa 594 (R_0=5.4 nm)[c]	Cy3B/ Abberior* 635 (R_0 = 5.9 nm)[c]	Alexa 488	Alexa 594	Alexa 488/ Alexa 594 (R_0 = 5.4 nm)[c]	Cy3B/ Abberior*635 (R_0 = 5.9 nm)[c]	Atto 550/ Atto 647N (R_0 = 6.6 nm)[c]
-1C, S89C, V104C, I113C, A151C, T161C,	-1C, S89C	-1C/113C, -1C/G194C, V104C/G194C, I113C/G194C	V104C/G194C	D110C	D2C, E56C, D110C	I113C/G194C, D2C/E56C, E56C/D110C, D2C/D110C	E56C/D110C	E56C/D110C

Extended Data Table 2.

Binding affinities, molecular dimensions, and reconfiguration times of fluorescently labeled H1 and ProTα.(top left) Affinities of labeled ProTα for H1 at different ionic strength (IS) and for H1 fragments for 165 mM IS ([b]see Extended Data Table 1). Uncertainties for the IS dependence are standard errors estimated from two independent titrations ([a]uncertainty at 165 mM: see Methods), for fragment binding from dilution errors (see Methods). [c]Apparent K_D from fraction of all bound species. **(top center)** Binding affinities of ProTα and H1 labeled with different dye pairs for the respective unlabeled partner. dUncertainties based on dilution errors. (top right) Transfer efficiencies and average distances of ProTα and H1 labeled with different dye pairs in the bound (R_{bound}) and unbound state ($R_{unbound}$). Uncertainties in distance are based on an estimated systematic error of ± 0.05 in the transfer efficiency from instrument calibration for the different dye pairs. **(bottom left)** Intermolecular reconfiguration times for the complex of donor-labeled H1

and acceptor-labeled ProTα and *vice versa*. **(bottom right)** Reconfiguration times of doubly labeled ProTα and H1 (unbound and bound). Uncertainties estimated by propagating the error on the transfer efficiency (± 0.05).

Affinity in TBS 165 mM (ProTα 56/110 Alexa 488/Alexa 594)				Affinity in TBS 205 mM		Intramolecular transfer efficiencies and distances in TBS 205 mM				
Ionic strength (mM)	**K_D (nM)**	**H1 fragm.**	**K_D**	**ProTα**	**[d]K_D (nM)**	**ProTα**	**$E_{unbound}$**	**E_{bound}**	**$R_{unbound}$ (nm)**	**R_{bound} (nm)**
[a]**165**	$(2.1^{+1.1}_{-0.8})\cdot10^{-3}$	[b]CTR	40^{+6}_{-4} pM	D2C/D110C Alexa 488/594	2.0 ± 0.13	E56C/D110C Alexa 488/59	0.36	0.54	$7.5^{+1.0}_{-0.3}$	$5.8^{+0.7}_{-0.1}$
180	$(37 \pm 5)\cdot10^{-3}$					E56C/D110C Cy3B/Abb.*635	0.41	0.56	$7.6^{+0.6}_{-0.5}$	6.2± 0.4
205	1.0 ± 0.1	[b]NTR	173^{+29}_{-28} nM	E56C/D110C Cy3B/Abb.*635	1.0 ± 0.10	E56C/D110C Atto 550/647N	0.45	0.59	$8.1^{+0.6}_{-0.5}$	$6.7^{+0.5}_{-0.4}$
240	26 ± 3			E56C/D110C Atto 550/647N	3.1 ± 0.20	V104C/G194C Cy3B/Abb.*635	0.18	0.52	$11.6^{+1.8}_{-1.2}$	$6.5^{+0.5}_{-0.4}$
290	$(2.5 \pm 2.1)\cdot10^{2}$	[b]GD	$1.9^{+0.3}_{-0.3}$ µM[c]	H1		H1	In TBS 165 mM			
						D2C/D110C Alexa 488/594	0.18	0.33	$10.6^{+1.6}_{-1.1}$	$7.9^{+0.7}_{-0.6}$
330	$(1.4 \pm 0.4)\cdot10^{3}$			V104C/G194C Alexa 488/594	3.5 ± 0.23	I113C/G194C Alexa 488/594	0.23	0.58	$9.5^{+1.1}_{-0.9}$	5.5± 0.4
340	$(4.0 \pm 1.8)\cdot10^{3}$					V104C/G194C Alexa 488/594	0.14	0.52	$11.4^{+2.1}_{-1.4}$	5.9± 0.4

ProTα / A-594 — H1 / A-488	τ_r (ns) D2C	τ_r (ns) E56C	τ_r (ns) D110C	Labeled Protein (Alexa 488/ Alexa 594)	τ_r (ns) unbound	τ_r (ns) bound
H1-1C	180^{+19}_{-16}	191^{+22}_{-19}	169^{+19}_{-16}	ProTα E56C/D110C	29±2	102^{+3}_{-2}
H1 I113C	121^{+13}_{-11}					
H1 A151C	124^{+13}_{-12}	98^{+16}_{-2}		ProTα D2C/D110C	33±2	66±2
H1 G194C	156^{+16}_{-14}		142^{+19}_{-15}			
A-488 / A-594				ProTα D2C/D110C	78^{+15}_{-9}	133^{+10}_{-7}
H1 G194C			120^{+13}_{-12}	H1	118^{+24}_{-14}	143^{+5}_{-4}

Supplementary Material

Refer to Web version on PubMed Central for supplementary material.

Acknowledgements

We thank Signe A. Sjørup and Jacob Hertz Martinsen for purification assistance, Andreas Prestel and Micha B. Kunze for helpful NMR advice, Erik Holmstrom for help with data analysis, Davide Mercadante for assistance with electrostatics calculations, Rodrigo Sobrino for help with the characterization of the H1-ProTα interaction in the early stages of the project, and Julie Forman-Kay, Martin Blackledge, Rohit Pappu, and Alex Holehouse for valuable discussions. This work was supported by the Swiss National Science Foundation (B.S.), the Danish Research Council (B.B.K/# 4181-00344), the Novo Nordisk Foundation (B.B.K and P.O.H), the Carlsberg Foundation (P.O.H.), and the intramural research program of the National Institute of Diabetes and Digestive and Kidney Diseases of the National Institutes of Health (R.B.B.). This work utilized the computational resources of the NIH HPC Biowulf cluster (http://hpc.nih.gov).

References

1. Wright PE & Dyson HJ Linking folding and binding. Curr. Opin. Struct. Biol 19, 31–38 (2009). [PubMed: 19157855]
2. Habchi J, Tompa P, Longhi S & Uversky VN Introducing protein intrinsic disorder. Chem Rev 114, 6561–6588 (2014). [PubMed: 24739139]
3. Tompa P & Fuxreiter M Fuzzy complexes: polymorphism and structural disorder in protein-protein interactions. Trends in biochemical sciences 33, 2–8 (2008). [PubMed: 18054235]
4. Baker JM et al. CFTR regulatory region interacts with NBD1 predominantly via multiple transient helices. Nat. Struct. Mol. Biol 14, 738–745 (2007). [PubMed: 17660831]
5. Mittag T et al. Dynamic equilibrium engagement of a polyvalent ligand with a single-site receptor. Proc. Natl. Acad. Sci. U. S. A 105, 17772–17777 (2008). [PubMed: 19008353]
6. Hendus-Altenburger R et al. The human Na(+)/H(+) exchanger 1 is a membrane scaffold protein for extracellular signal-regulated kinase 2. BMC Biol 14, 31 (2016). [PubMed: 27083547]
7. Milles S et al. Plasticity of an Ultrafast Interaction between Nucleoporins and Nuclear Transport Receptors. Cell 163, 734–745 (2015). [PubMed: 26456112]
8. Csizmok V, Follis AV, Kriwacki RW & Forman-Kay JD Dynamic Protein Interaction Networks and New Structural Paradigms in Signaling. Chem. Rev 116, 6424–6462 (2016). [PubMed: 26922996]
9. Banani SF, Lee HO, Hyman AA & Rosen MK Biomolecular condensates: organizers of cellular biochemistry. Nat. Rev. Mol. Cell. Biol 18, 285–298 (2017). [PubMed: 28225081]
10. Robinson PJ & Rhodes D Structure of the '30 nm' chromatin fibre: a key role for the linker histone. Curr. Opin. Struct. Biol 16, 336–343 (2006). [PubMed: 16714106]
11. Hergeth SP & Schneider R The H1 linker histones: multifunctional proteins beyond the nucleosomal core particle. EMBO Rep 16, 1439–1453 (2015). [PubMed: 26474902]
12. Hansen JC, Lu X, Ross ED & Woody RW Intrinsic protein disorder, amino acid composition, and histone terminal domains. J. Biol. Chem 281, 1853–1856 (2006). [PubMed: 16301309]
13. Gast K et al. Prothymosin alpha: a biologically active protein with random coil conformation. Biochemistry 34, 13211–13218 (1995). [PubMed: 7548085]
14. Uversky VN et al. Natively unfolded human prothymosin alpha adopts partially folded collapsed conformation at acidic pH. Biochemistry 38, 15009–15016 (1999). [PubMed: 10555983]
15. Gomez-Marquez J & Rodriguez P Prothymosin alpha is a chromatin-remodelling protein in mammalian cells. Biochem. J 333, 1–3 (1998). [PubMed: 9639554]
16. Mosoian A Intracellular and extracellular cytokine-like functions of prothymosin alpha: implications for the development of immunotherapies. Future Med. Chem 3, 1199–1208 (2011). [PubMed: 21806381]
17. George EM & Brown DT Prothymosin alpha is a component of a linker histone chaperone. FEBS letters 584, 2833–2836 (2010). [PubMed: 20434447]

18. Papamarcaki T & Tsolas O Prothymosin alpha binds to histone H1 in vitro. FEBS letters 345, 71–75 (1994). [PubMed: 8194604]
19. Barbero JL, Franco L, Montero F & Moran F Structural Studies on Histones-H1 - Circular-Dichroism and Difference Spectroscopy of the Histones-H1 and Their Trypsin-Resistant Cores from Calf Thymus and from the Fruit-Fly Ceratitis-Capitata. Biochemistry 19, 4080–4087 (1980). [PubMed: 7190838]
20. Ramakrishnan V, Finch JT, Graziano V, Lee PL & Sweet RM Crystal-Structure of Globular Domain of Histone H5 and Its Implications for Nucleosome Binding. Nature 362, 219–223 (1993). [PubMed: 8384699]
21. Yi S, Brickenden A & Choy WY A new protocol for high-yield purification of recombinant human prothymosin alpha expressed in Escherichia coli for NMR studies. Protein expression and purification 57, 1–8 (2008). [PubMed: 17949994]
22. Khan H et al. Fuzzy complex formation between the intrinsically disordered prothymosin alpha and the Kelch domain of Keap1 involved in the oxidative stress response. Journal of molecular biology 425, 1011–1027 (2013). [PubMed: 23318954]
23. Zhou BR et al. Structural insights into the histone H1-nucleosome complex. Proc. Natl. Acad. Sci. U. S. A 110, 19390–19395 (2013). [PubMed: 24218562]
24. Zarbock J, Clore GM & Gronenborn AM Nuclear magnetic resonance study of the globular domain of chicken histone H5: resonance assignment and secondary structure. Proc. Natl. Acad. Sci. U. S. A 83, 7628–7632 (1986). [PubMed: 3463990]
25. Kjaergaard M, Brander S & Poulsen FM Random coil chemical shift for intrinsically disordered proteins: effects of temperature and pH. J Biomol NMR 49, 139–149 (2011). [PubMed: 21234644]
26. Bae SH, Dyson HJ & Wright PE Prediction of the rotational tumbling time for proteins with disordered segments. J. Am. Chem. Soc 131, 6814–6821 (2009). [PubMed: 19391622]
27. Schuler B, Hofmann H, Soranno A & Nettels D Single-molecule FRET spectroscopy and the polymer physics of unfolded and intrinsically disordered proteins. Annu. Rev. Biophys 45, 207–231 (2016). [PubMed: 27145874]
28. Sisamakis E, Valeri A, Kalinin S, Rothwell PJ & Seidel CAM Accurate Single-Molecule FRET Studies Using Multiparameter Fluorescence Detection. Methods Enzymol 475, 455–514 (2010). [PubMed: 20627168]
29. Müller-Späth S et al. Charge interactions can dominate the dimensions of intrinsically disordered proteins. Proc. Natl. Acad. Sci. U. S. A. 107, 14609–14614 (2010). [PubMed: 20639465]
30. Hofmann H et al. Polymer scaling laws of unfolded and intrinsically disordered proteins quantified with single-molecule spectroscopy. Proc. Natl. Acad. Sci. U. S. A 109, 16155–16160 (2012). [PubMed: 22984159]
31. White AE, Hieb AR & Luger K A quantitative investigation of linker histone interactions with nucleosomes and chromatin. Scientific reports 6, 19122 (2016). [PubMed: 26750377]
32. Pak CW et al. Sequence Determinants of Intracellular Phase Separation by Complex Coacervation of a Disordered Protein. Mol. Cell 63, 72–85 (2016). [PubMed: 27392146]
33. Chung HS, Louis JM & Gopich IV Analysis of Fluorescence Lifetime and Energy Transfer Efficiency in Single-Molecule Photon Trajectories of Fast-Folding Proteins. J. Phys. Chem. B 120, 680–699 (2016). [PubMed: 26812046]
34. Soranno A et al. Quantifying internal friction in unfolded and intrinsically disordered proteins with single molecule spectroscopy. Proc. Natl. Acad. Sci. U. S. A 109, 17800–17806 (2012). [PubMed: 22492978]
35. Nettels D, Gopich IV, Hoffmann A & Schuler B Ultrafast dynamics of protein collapse from single-molecule photon statistics. Proc. Natl. Acad. Sci. U. S. A 104, 2655–2660 (2007). [PubMed: 17301233]
36. Soranno A et al. Integrated view of internal friction in unfolded proteins from single-molecule FRET, contact quenching, theory, and simulations. Proc. Natl. Acad. Sci. U. S. A 114, E1833–E1839 (2017). [PubMed: 28223518]
37. Creigthon TE Proteins: structures and molecular properties. 2nd EditionPK edn, (W. H. Freeman and Company, 1993).

38. Karanicolas J & Brooks CL The origins of asymmetry in the folding transition states of protein L and protein G. Prot. Sci 11, 2351–2361 (2002).
39. Shoemaker BA, Portman JJ & Wolynes PG Speeding molecular recognition by using the folding funnel: the fly-casting mechanism. Proc. Natl. Acad. Sci. U. S. A 97, 8868–8873 (2000). [PubMed: 10908673]
40. Schreiber G, Haran G & Zhou HX Fundamental Aspects of Protein-Protein Association Kinetics. Chem. Rev. 109, 839–860 (2009). [PubMed: 19196002]
41. Borg M et al. Polyelectrostatic interactions of disordered ligands suggest a physical basis for ultrasensitivity. Proc. Natl. Acad. Sci. U. S. A 104, 9650–9655 (2007). [PubMed: 17522259]
42. Srivastava S & Tirrell MV Polyelectrolyte Complexation. Advances in Chemical Physics 161, 499–544 (2016).
43. Ahmad A et al. Heat shock protein 70 kDa chaperone/DnaJ cochaperone complex employs an unusual dynamic interface. Proc. Natl. Acad. Sci. U. S. A 108, 18966–18971 (2011). [PubMed: 22065753]
44. Freeman Rosenzweig ES et al. The Eukaryotic CO2-Concentrating Organelle Is Liquid-like and Exhibits Dynamic Reorganization. Cell 171, 148–162 e119 (2017). [PubMed: 28938114]
45. Nott TJ et al. Phase transition of a disordered nuage protein generates environmentally responsive membraneless organelles. Mol. Cell 57, 936–947 (2015). [PubMed: 25747659]
46. Vemon RM et al. Pi-Pi Contacts: An Overlooked Protein Feature Relevant To Phase Separation. (submitted).
47. Peng B & Muthukumar M Modeling competitive substitution in a polyelectrolyte complex. J. Chem. Phys 143, 243133 (2015). [PubMed: 26723618]
48. Berlow RB, Dyson HJ & Wright PE Hypersensitive termination of the hypoxic response by a disordered protein switch. Nature 543, 447–451 (2017). [PubMed: 28273070]
49. Wang D et al. Acetylation-regulated interaction between p53 and SET reveals a widespread regulatory mode. Nature 538, 118–122 (2016). [PubMed: 27626385]
50. Dosztanyi Z, Csizmok V, Tompa P & Simon I IUPred: web server for the prediction of intrinsically unstructured regions of proteins based on estimated energy content. Bioinformatics 21, 3433–3434 (2005). [PubMed: 15955779]
51. Record MT, Jr., Anderson CF & Lohman TM Thermodynamic analysis of ion effects on the binding and conformational equilibria of proteins and nucleic acids: the roles of ion association or release, screening, and ion effects on water activity. Q. Rev. Biophys 11, 103–178 (1978). [PubMed: 353875]
71. Kapanidis AN. et al. Alternating-laser excitation of single molecules. Acc. Chem. Res 38, 523–533 (2005). [PubMed: 16028886]
72. Hoffmann A et al. Mapping protein collapse with single-molecule fluorescence and kinetic synchrotron radiation circular dichroism spectroscopy. Proc. Natl. Acad. Sci. U. S. A 104, 105–110 (2007 [PubMed: 17185422]

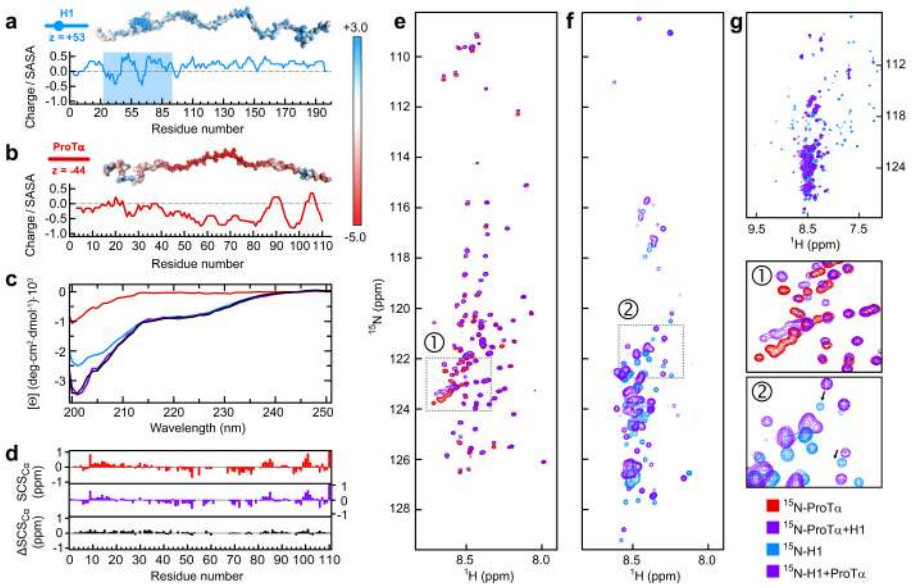

Figure 1. ProTα and H1 remain unstructured upon binding.

Extended configurations of H1 **(a)** and ProTα **(b)**, net charges, and surface electrostatic potentials with color scale (units in $k_B T/e$). For the globular domain of H1, only residues with a solvent-accessible surface area (SASA) > 0.5 nm^2 are included (cf. Extended Data Table 1). **(c)** Far-UV CD spectra of ProTα (red), H1 (blue), the ProTα-H1 mixture (purple), and their calculated sum (black) at 5 μM for each protein. **(d)** C^{α} secondary chemical shifts ($SCS_{c\alpha}$) of ProTα free (red), in complex with H1 (purple), and their differences (black). **(e)** $^{1}H,^{15}N$-HSQC spectra of ^{15}N-ProTα in the absence (red) and presence (purple) of unlabeled H1 and **(f)** ^{15}N-H1 in the absence (blue) and presence (purple) of unlabeled ProTα with zooms (①,②). **(g)** H1 spectra from (f) at lower contour level.

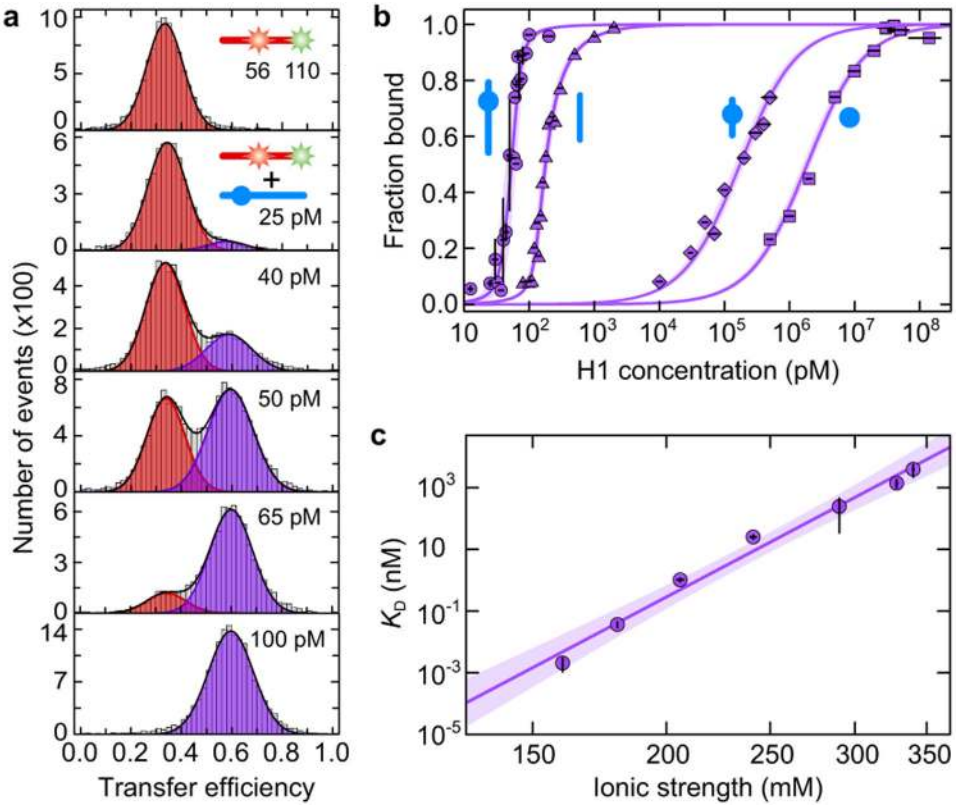

Figure 2. ProTα and H1 form an electrostatically driven high-affinity complex.

(a) Single-molecule transfer efficiency histograms of FRET-labeled ProTα (positions 56 and 110) without (top) and with increasing concentrations of unlabeled H1 as indicated in the panels, fitted with two peaks, unbound (red) and bound (purple). **(b)** Binding isotherms based on transfer efficiency histograms for full-length H1 (

, $K_D = 2.1^{+1.1}_{-0.8}$pM), N- (

, $K_D = 173^{+29}_{-28}$nM) and C-terminal (

, $K_D = 40^{+6}_{-4}$pM) regions, andthe globular domain of HI (

, $K_D = 1.9^{+0.3}_{-0.3}$μM) at 165 mM ionic strength (see Extended Data Table 1 for details). **(c)** K_D of H1-ProTα complex as a function of ionic strength with fit51 (purple line) and 95% confidence interval (shaded). See Methods for details of data analysis.

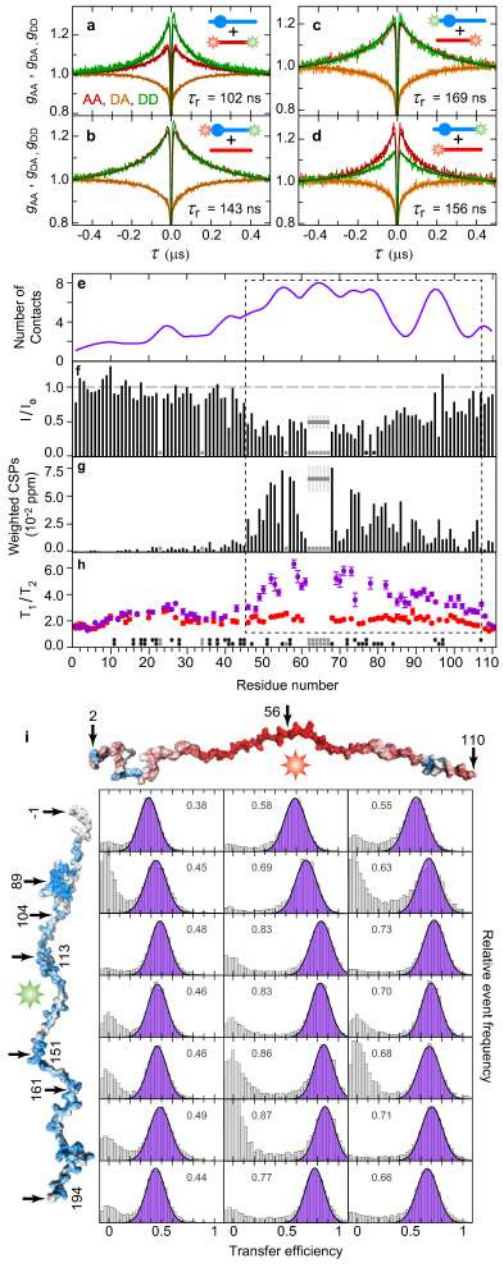

Figure 3. Dynamics, interactions, and distances in the complex.

(a-d) Examples of nsFCS probing long-range dynamics based on intra- and intermolecular FRET (see Extended Data Table 2 for details). **(e)** Average number of contacts of each ProTα residue with H1 based on the simulations (Fig. 4b). **(f)** Ratios of NMR resonance intensities of ProTα in the presence *(I)* and absence (I_0) of H1. **(g)** Weighted backbone amide chemical shift perturbations (CSPs) of ProTα induced by equimolar H1 binding (see Extended Data Fig. 2 for other stoichiometries). In (f-g), the grey horizontal lines represent the average of three unassigned but traceable Glu residues in the range 62-67 with error bars from their standard deviation (see Methods for details). **(h)** Ratios of longitudinal (T_1) and transverse (T_2) ^{15}N relaxation times of ProTα in the free (red) and bound (purple) states (see

Extended Data Fig. 2 for details). Light grey stars indicate prolines and unassigned residues, dark grey stars resonance overlap and/or insufficient data quality. The dashed box indicates the sequence range with the largest changes. **(i)** Transfer efficiency (*E*) histograms from intermolecular single-molecule FRET experiments between different positions in ProTα and H1, fitted with a single peak (purple, *E* values shown). The signal at $E \approx 0$ originates from molecules without FRET acceptor.

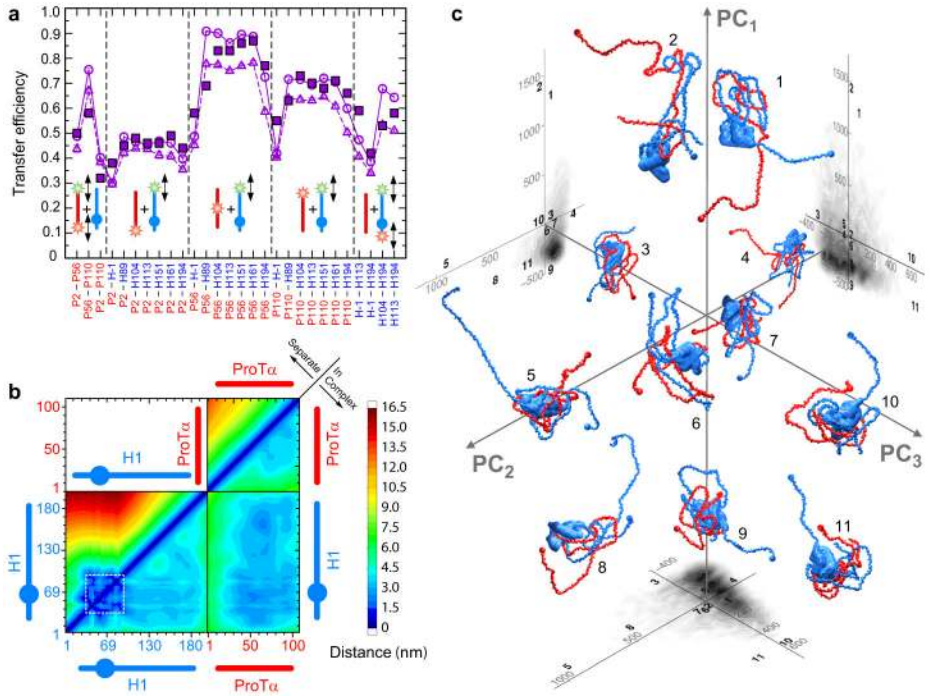

Figure 4. Architecture of the complex from simulations.

(a) Comparison of experimental (filled squares) and simulated transfer efficiencies (empty symbols) in the H1-ProTα complex for the pairs of dye positions indicated below (triangles and circles: simulations with and without explicit chromophores, respectively). **(b)** Intra- and intermolecular average distance maps of H1 and ProTα from the simulations, separately and in the complex. The white dashed square indicates the globular domain (only surface-exposed residues shown, see Extended Data Table 1). **(c)** Examples of conformations of H1 (blue) and ProTα (red) in the complex; the N-termini are indicated by small spheres. The structures are projected onto the first three principal components (PC) of the distance map, with projections of the full ensemble shown as gray scatter plots (units of Å, see also Extended Data Fig. 6). Numbers indicate the positions of the structures in the PC projections.